Mingo, B.; Mohedano, M.; Blawert, C.; del Olmo, R.; Hort, N.; Arrabal, R.:

Role of Ca on the corrosion resistance of Mg–9Al and Mg–9Al–0.5Mn alloys.

In: Journal of Alloys and Compounds. Vol. 811 (2019) 151992.
First published online by Elsevier: 23.08.2019

https://dx.doi.org/10.1016/j.jallcom.2019.151992

Role of Ca on the corrosion resistance of Mg-9Al and Mg-9Al-0.5Mn alloys

B. Mingo[a*], M. Mohedano[b], C. Blawert[c], R. del Olmo[b], N. Hort[c], R. Arrabal[b]

[a] *School of Materials, University of Manchester, Oxford Road, Manchester, M13 9PL, UK*

[b] *Department of Chemical and Materials Engineering, Faculty of Chemistry, Complutense University of Madrid, 28040, Spain*

[c] *Magnesium Innovation Centre, Helmholtz-Zentrum Geesthacht, 21502 Geesthacht, Germany*

[*]*Corresponding author*

E-mail: beatriz.mingo@manchester.ac.uk

ABSTRACT

The effect of Ca additions on the microstructure and corrosion resistance of Mg-9Al and Mg-9Al-0.5Mn alloys is investigated. Model alloys were used instead of a commercial AZ91 alloy in order to avoid masking effects from other alloying elements. Grain size and secondary phases were characterised with special interest in their Volta potential. Corrosion performance was evaluated by hydrogen evolution and electrochemical methods. A synergetic effect was found when Ca and Mn were added in small amounts (0.5 wt.%), reaching corrosion rates up to two orders of magnitude lower than the model Mg-9Al alloy. Such improvement was associated with Ca decreasing the Volta potential of the β-phase and with Ca and Mn decreasing the galvanic activity of Fe-rich intermetallics. Precipitation of Al_2Ca decreased the amount of β-phase and had a negative impact on the corrosion resistance due to its cathodic behaviour.

KEYWORDS: Magnesium; Calcium; Manganese; Alloying, Corrosion; Volta potential

1. Introduction

Worldwide Mg production has steeply grown during the last decades. From 1991 to 2016, the total production of primary magnesium has increased from 131 to 1010 thousand metric tons [1]. Such growth is mainly driven by the transport sector due to the current need to produce more energy efficient vehicles. However, the poor corrosion resistance of this metal still represents a great challenge that limits its full implementation.

Surface modification is a common practice to increase the corrosion resistance of magnesium alloys. For instance, surface modification by machine hammer peening and burnishing [2] or the application of coatings by conversion methods [3], plasma electrolytic oxidation [4] or thermal spraying [5], amongst others, result in a considerably increase of the corrosion performance of magnesium alloys. However, these techniques require a second step on the manufacturing process, with the consequent increase in the processing time and cost. Alloy design allows modifying the microstructure of the alloys and, therefore, the mechanical and corrosion performance, just by incorporating specific amounts of alloying elements to the cast melt. It is the most fundamental method used to develop new alloys, due to the simplicity and low cost of the process.

The incorporation of Al as an alloying element is almost mandatory for those applications where castability, enhanced strength and corrosion resistance are required. The positive effect of Al lies in its capacity to improve the protective properties of the pseudo-passive layer naturally formed on the metal surface [6]. The formation of the β-$Mg_{17}Al_{12}$ phase (commonly known as β-phase) is also important, although its positive or negative influence depends on several factors [7]. In general terms, interconnected β-phase improves the corrosion resistance by the so-called barrier effect, whereas isolated particles can be detrimental by forming active galvanic couples [8]. Previous

studies by the authors have revealed that the composition of the β-phase also plays a fundamental role on its overall effect from a corrosion point of view. For instance, it was observed in [9] that Ca and Sn can be incorporated into the β-phase, thus decreasing or increasing, respectively, the Volta potential of the β-phase. This, in turn, resulted in significant changes in the measured corrosion rate.

Although the corrosion resistance of commercially pure Mg is improved with the addition of Al, this is still not enough for critical components. Fe impurities, which are very common in cast alloys, are extremely detrimental because they readily form micro-galvanic couples with the Mg matrix [7]. Mn has traditionally been used as Fe scavenger; it replaces Fe and Al-Fe intermetallics by less detrimental Al-Mn-Fe particles. However, if added in high amounts, Mn leads to excessive formation of cathodic Al-Mn particles (Al_8Mn_5, Al_6Mn, Al_5Mn_2 or Al_4Mn) [6]. It has been reported repeatedly that the optimum amount of Mn shall be such that the Fe/Mn ratio does not exceed 0.032 [10-12], however, the exact ratio depends on alloy composition and processing [9, 13, 14].

Over the last decade, there has been an increased interest in fine-tuning of the composition of Mg-Al alloys, which are the most commonly used Mg alloys [15-17]. Most of them are concerned with the refinement of the β-phase [18, 19] and/or the effect of new intermetallic phases [17, 20, 21]. However, very few of them mentioned the compositional modification of the β-phase and its impact from a corrosion point of view [22, 23]. Zhou *et al.* [22] studied the influence of Ca additions (<1 wt. %), reporting a positive influence on the corrosion resistance of AZ91 alloy. They identified the presence of Ca within the β-phase, however they did not correlate this with the ability of Ca to decrease its galvanic coupling with the α-Mg matrix. Nam *et al.* [23] studied the

influence of CaO additions into alloy AZ91 and also observed Ca enrichment of the β-phase. However, they just attributed the improvement to the better protective properties of the passive layer. Dabah [18] studied the effect of Ca incorporations (0.9-1.8 wt %) in a Mg-5Al alloy and associated the improvement with Ca refining the β-phase. Apachitei [24] characterised the Volta potential difference of micro-constituents in a Mg-Al-Ca alloy by scanning Kelvin probe force microscopy, but they did not mention the effect of Ca on the β-phase composition and/or morphology. This evidences that further research is required where a clear interconnection of these phenomena is stablished.

In this work, Mg-9Al and Mg-9Al-0.5Mn model alloys were modified with 0.5, 1.0 and 2.0 wt.% Ca, with the aim of understanding the role of this element on the corrosion resistance of Mg-Al alloys, with and without the presence of Mn. This research, for the first time, correlates microstructure refinement, secondary phase composition modification, area fraction and Volta potential with the corrosion behaviour of Ca modified Mg-Al alloys. Grain size and secondary phases were characterised with special interest in their electrochemical activity, analysed by Scanning Kelvin Probe Force Microscopy (SKPFM). Corrosion resistance was evaluated by hydrogen collection and electrochemical methods.

2. Materials and methods

2.1. Test materials

The alloys were fabricated at the Magnesium Innovation Centre (Helmholtz Zentrum Geesthacht, Germany) by gravity casting using a finger mould (Ø=18 mm). During the casting, a protective atmosphere (Ar, 0.2 vol. % SF_6) was used to prevent oxidation. Mg was molten at 680 °C and the

alloying elements (Mn and Ca) were incorporated to the melt as elemental additions. Spark optical emission spectroscopy (Spectrolab, Spectro, Kleve) was used to determine the chemical composition of the alloys (Table 1). The total amount of alloying elements was selected according to previous results obtained in [9]. Specimens of 1.8 cm of diameter and 0.5 cm of thickness were cut from the ingot.

2.2. Characterisation

Specimens were ground using successive grades of silicon carbide paper (up to P1200) and polished with diamond paste (up to 0.1 μm) using an alcohol based lubricant. The microstructure was revealed after chemical etching with acetic-picral solution (5 g picric acid, 100 mL ethanol, 5 mL acetic acid and 10 mL water) and the grain size was determined using the Heyn or lineal method [25]. Optical micrographs were acquired under polarized light at arbitrary locations using a Leica DM LM optical microscope. Specimens were also characterised using a JEOL JSM-6400 scanning electron microscopy (SEM) equipped with energy dispersive X-ray (EDS) microanalysis spectrometer (Oxford Link PENTAFET 6506).

Specimens were further characterised by X-ray diffraction (XRD) using a Philips X'Pert diffractometer (Cu Kα = 1.54056 Å). A Bragg-Brentano geometry, in the 2θ range 10-90°, with a step size of 0.04° and a dwell time of 5 s per step was used. XRD patterns were analysed with the software PANalytical's X'Pert High Score and the ICDD PDF-4+ database.

Phase quantification studies were carried out by image analysis on at least three backscattered scanning electron micrographs taken at ×200 using the ImageJ software.

Micro-constituent of each alloy was analysed by scanning Kelvin probe force microscopy (SKPFM) using a NanoscopeIIIa MultiMode instrument (Veeco-Digital Instruments) and a Si tip

coated with a thin layer of Pt (20 nm) working in tapping mode. Surface or Volta potential maps were acquired using the two-pass technique [8] maintaining a constant distance between the tip and the sample (100 nm). The specimens were polished 24 h prior the measurement and kept in a desiccator to prevent partial oxidation. All measurements were carried out at 22 ºC and a relative humidity in the range of 40-65 %. The experimental data was analysed using WSXM software [26]. The provided Volta potential difference values refer to the electrostatic potential difference between the phase of interest and the surrounding magnesium matrix.

SKPFM is a powerful technique that can be used to predict micro galvanic couples; however, there are some limitations that need to be considered when using this technique to assess the corrosion resistance of metallic materials. SKPFM provides the Volta potential of microconstituents in air, opposite to corrosion, that takes place in the presence of an electrolyte. Therefore, it does not account for the influence of the media, which is a key factor on the corrosion resistance of any material. Additionally, it does not account for the kinetics of the anodic/cathodic reactions, since it is a purely thermodynamic parameter. Hence, Volta potentials measured by SKPFM should be analysed with caution as they only indicate the expected relative driving force for microgalvanic coupling [27]. In previous works a correlation between the Volta potential measured with SKPFM and electrode potential in solution was established for the most common intermetallic phases present in magnesium alloys in neutral NaCl solutions [27, 28]. This suggests that SKPFM is a suitable technique to predict the electrochemical behaviour of secondary phases in the Mg-Al system.

2.3. Corrosion tests

Hydrogen evolution tests were performed in triplicate using 1 cm^2 ground specimens. Measurements were carried out during 3 and 14 days of immersion in naturally-aerated 0.5 wt. %

NaCl solution depending on the performance of each alloy. From the total volume of H_2 evolved during the cathodic reaction, the mass of dissolved Mg was calculated using the following formula $m_{Mg} = 1.085\, V_{H_2}$ [29]. A scheme of the experimental set-up can be found in [30].

Potentiodynamic polarisation curves were recorded using a GillAC potentiostat (ACM Instruments) and a three-electrode cell, where the specimen (1cm^2) acts as the working electrode and graphite and Ag/AgCl (0.210 V *vs*. SHE) electrodes serve as counter and reference electrodes, respectively. Both cathodic and anodic branches were acquired separately. The cathodic one was recorded from −150 mV *vs*. the open circuit potential (OCP) and the anodic branch from the OCP until a maximum current of 5 mA/cm^2 using a scan rate of 0.3 mV/s. Tafel extrapolation of the cathodic branch was used to calculate the corrosion current density.

Early stages of corrosion were investigated after immersion of polished (0.25 μm diamond finish) and etched (2 s in 1% nital) specimens in 0.5 wt. % NaCl for 10 min. After the test, specimens were examined with an optical 3D measurement system based on focus-variation technology (InfiniteFocusSL, Alicona Imaging GmbH).

3. Results and discussion

3.1. Alloy characterisation

Figure 1 shows optical micrographs of the studied magnesium alloys under polarized light; the reference Mg-9Al alloy, three Ca-containing alloys (Mg-9Al-0.5Ca, Mg-9Al-1Ca, Mg-9Al-2Ca), one Mn-containing alloy (Mg-9Al-0.5Mn) and three Ca- and Mn-containing alloys (Mg-9Al-0.5Mn-0.5Ca, Mg-9Al-0.5Mn-1Ca and Mg-9Al-0.5Mn-2Ca). All of them show equiaxed-dendritic grains with sizes ranging from ~60 to 150 μm (Table 2). Variations in grain size were

attributed to differences in cooling rate and Al content between the alloys (Figure 1f). Some authors [31] have reported grain refinement in Mg-Al alloys modified with Ca. This effect is typically attributed to Ca segregation in the grain boundaries and precipitation of the Al_2Ca phase [32]. It has also been stated that that large Ca additions are less effective for grain refinement. For instance, Hirai *et al*. [33] observed that grain refinement in the AZ91 alloy was less significant for Ca additions above 1 wt.%. This is possibly related to precipitation of large amounts of Al_2Ca particles instead of the β-phase. It is important to note that many studies on Mg-Al alloys report grain refinement following alloying additions, including Ca, but do not provide grain size measurements based on micrographs under polarized light. This could be quite misleading and should be taken into consideration. Based on the present results, Ca does not act as a grain refiner in the studied alloys.

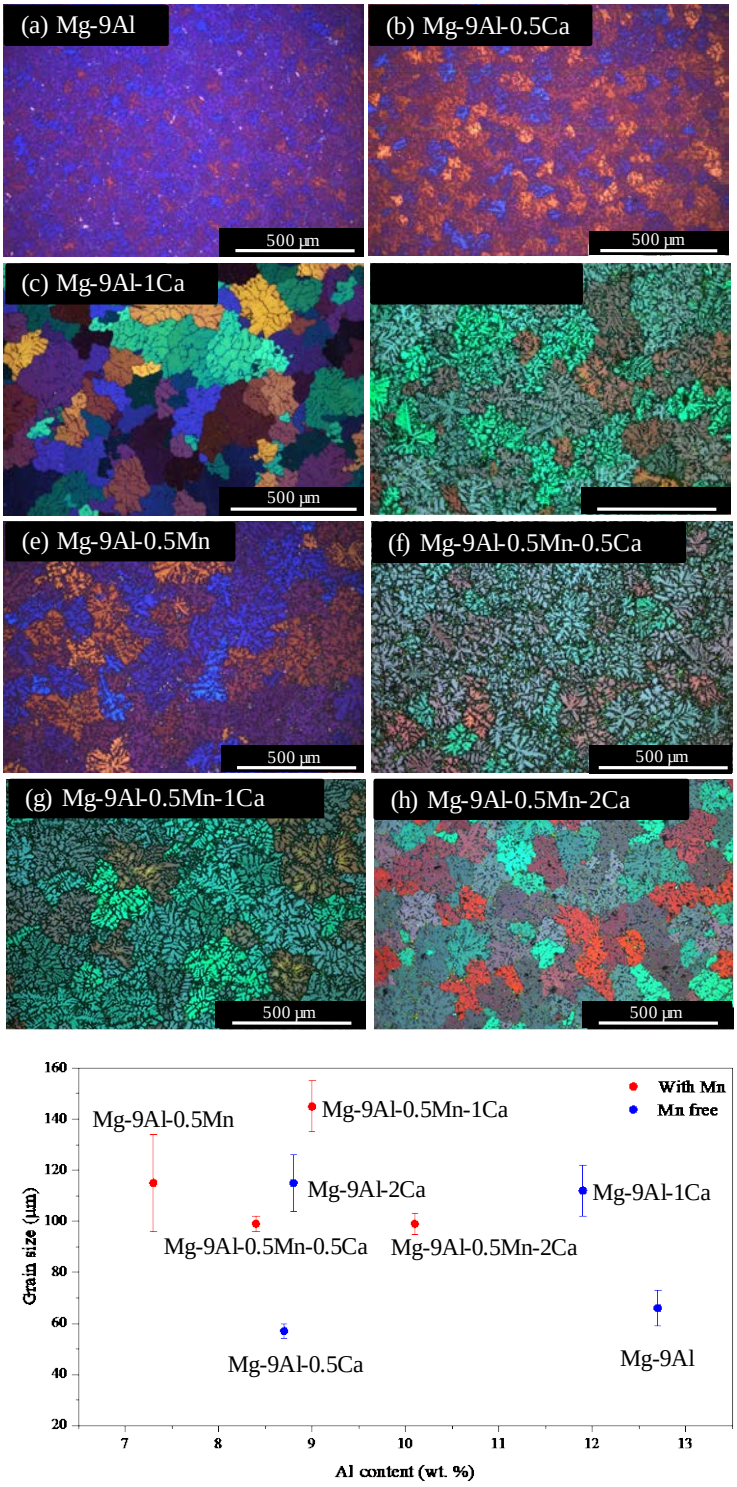
(a) Mg-9Al
500 μm
(b) Mg-9Al-0.5Ca
500 μm
(c) Mg-9Al-1Ca
500 μm
500 μm
(e) Mg-9Al-0.5Mn
500 μm
(f) Mg-9Al-0.5Mn-0.5Ca
500 μm
(g) Mg-9Al-0.5Mn-1Ca
500 μm
(h) Mg-9Al-0.5Mn-2Ca
500 μm
With Mn
Mn free
Mg-9Al-0.5Mn
Mg-9Al-0.5Mn-1Ca
Mg-9Al-2Ca
Mg-9Al-1Ca
Mg-9Al-0.5Mn-0.5Ca
Mg-9Al-0.5Mn-2Ca
Mg-9Al-0.5Ca
Mg-9Al
Grain size (μm)
Al content (wt. %)
160
140
120
100
80
60
40
20
7
8
9
10
11
12
13

Figure 1

Details of the microstructures of studied materials are shown in Figure 2. The Mg-9Al alloy (Figure 2a) shows primary α-Mg grains and a partially divorced eutectic (α-Mg/β-$Mg_{17}Al_{12}$) at the interdendritic regions. The latter is formed due to non-equilibrium solidification so that the last liquid to solidify reaches the eutectic composition. For the same reason, there is significant Al segregation within the α-Mg matrix; ~6 wt. % Al at the centre and ~13 wt. % Al at the surroundings of the eutectic. Al-Mn-Fe inclusions are also observed. Fe-rich impurities are quite common, even in model alloys, due to contamination from the steel crucible. The chemical compositions of studied phases are shown in Table 3.

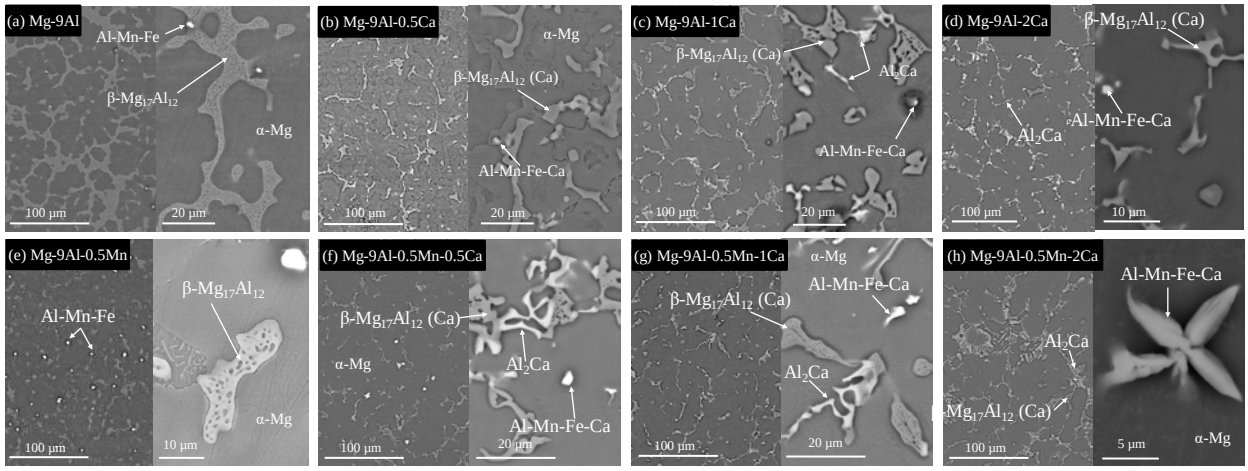

Figure 2.

The addition of Ca produces several microstructural modifications. EDS analysis revealed Ca incorporation into Fe-rich impurities and the β-phase (Table 3). The latter was also confirmed by XRD, where β-phase diffraction peaks shifted towards lower 2-theta values due to partial replacement of Al and Mg by larger Ca atoms (Figure 3). The addition of 1 and 2 wt.% Ca (Mg-9Al-1Ca and Mg-9Al-2Ca) resulted in precipitation of significant amounts of Al_2Ca (Figure 2c,d and Figure 3). This intermetallic shows a bone-like morphology and precipitates next to the β -phase. It is worth mentioning that the Al_2Ca phase was not identified in the Mg-9Al-0.5Ca alloy,

although it should be present according to the Mg-Al-Ca phase diagram included in [34]. This is probably related to a faster cooling rate for this alloy compared to Mg-9Al-1Ca and Mg-9Al-2Ca alloys. As a result, there is a greater incorporation of Ca atoms in the β-phase, as shown in the greater shift of XRD peaks for the β-phase (Figure 3b) and EDS analysis (Table 3). An additional evidence of a faster cooling rate is that the Mg-9Al-0.5Ca alloy shows a completely divorced eutectic (Figure 2b) instead of a partially divorced one (Figure 2c). Quantitative image analysis studies confirmed that the Al_2Ca area fraction generally increases with the total amount of Ca added to the alloy, resulting in a proportional decrease of β-phase (Figure 4).

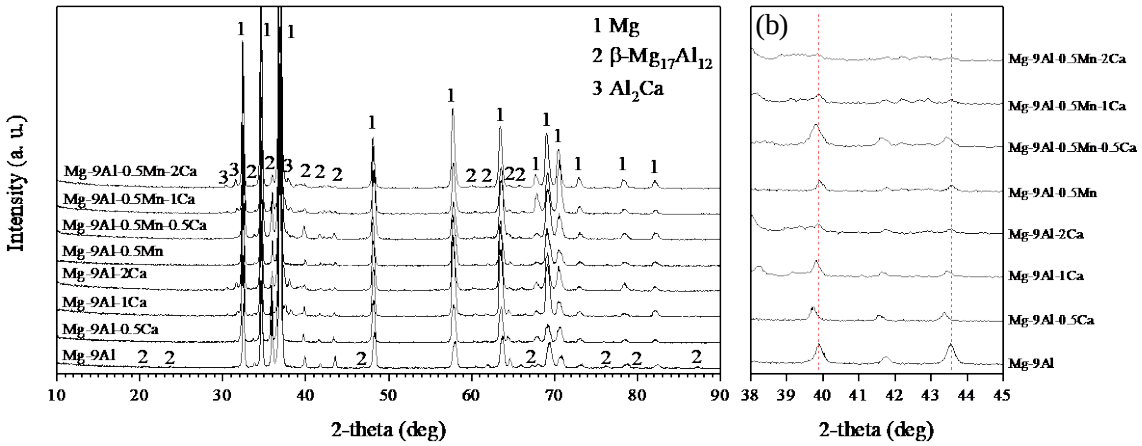

Figure 3

The Mg-9Al-0.5Mn alloy shows a similar microstructure when compared to the unmodified Mg-9Al alloy, although there is greater number of Al-Mn-Fe particles, due to its higher Mn content (Table 2). Also, these inclusions show a higher percentage of Mn, *i.e.*, ~54 *vs*. 1.5 wt. % Mn (Table 3).

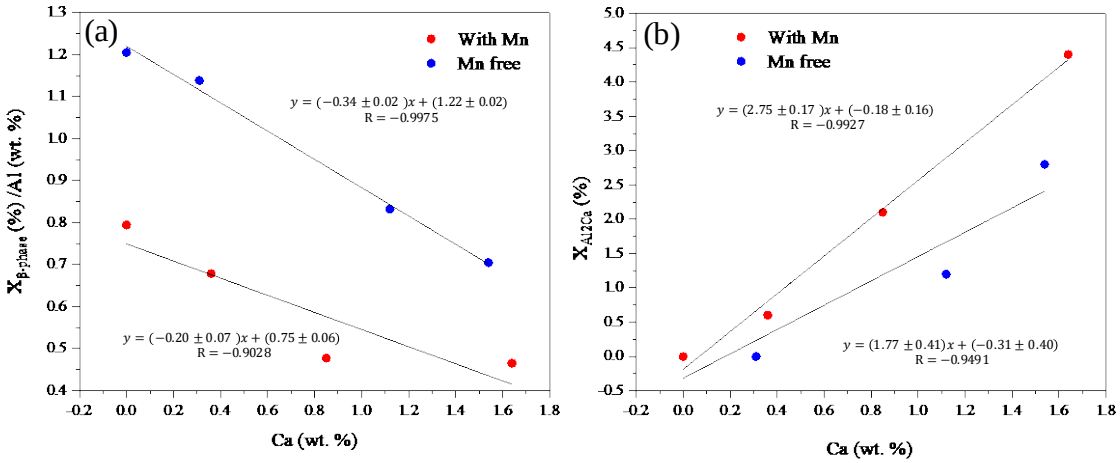

Figure 4

The incorporation of Ca into the Mg-9Al-0.5Mn alloy showed similar effects, as previously described for the Mg-9Al alloy; Ca is incorporated into the β-phase and Al-Mn-Fe phases, which in some cases show a star-shaped morphology, and an increased area fraction of Al_2Ca phase is measured with increasing Ca contents (Table 2, Figure 4b). It is worth mentioning that Ca had a negligible effect on the population density of Al-Mn-Fe inclusions, indicating that their number is mostly determined by the total amount of Mn in the alloy, *e.g.*, Mg-9Al-0.5Mn-1Ca shows a relatively high amount of these inclusions due to its higher Mn content (Tables 1 and 2).

Surface Volta potential maps of the studied alloys were obtained by SKPFM (Figure 5) with the aim of elucidating the electrochemical activity of each microconstituent. Table 4 compiles the surface Volta potential differences of all the phases identified in the studied alloys and shows that all the analysed particles are cathodic with respect to the α-Mg matrix. The β-phase in Mg-9Al and Mg-9Al-0.5Mn shows a Volta potential difference in the rage of 30-70 mV, which is comparable to those obtained in other works [35]. It is worth mentioning that some authors [36, 37] observed higher values, reaching Volta potential differences of ~ 260 mV in die cast AZ91 alloys. Such

discrepancy is related to compositional differences. Usually, die cast processes, where cooling rates are high, lead to the formation of a β-phase with higher aluminium content, and therefore with a higher Al/Mg ratio compared to gravity cast alloys. The incorporation of Ca into the β-phase decreased the Volta potential difference of this phase down to 15-25 mV in all Ca-containing alloys. This is due to the lower standard reduction potential of Ca (–2.868 V_{SHE}) compared to that of Al (−1.662 V_{SHE}) and Mg (−2.372 V_{SHE}).

The measured values for the Al_2Ca phase are relatively constant (60-70 mV) throughout the alloys and are similar to those obtained in other works [18, 24]. The Al-Mn-Fe rich inclusions show a wider range of values depending on the alloy. In case of Mg-9Al, measured values range between 250 and 700 mV, depending on their Fe content [9, 24]. The incorporation of Ca to these inclusions (Mg-9Al-0.5-2Ca) reduces the measured values considerably, laying in the range of 50-100 mV. Mg-9Al-0.5Mn alloy shows inclusions characterised by considerably lower Volta potential values (120-300 mV) compared to the unmodified alloy Mg-9Al, which can be explained by the higher proportion of Mn within the particles, which offsets the Fe negative effect (*scavenger effect*). The incorporation of Ca to Mn-containing alloys further reduces the Volta potential values of Fe-rich intermetallics (130-140 mV). The slightly higher figure of the latter, compared to Mn-free alloys (Mg-9Al-0.5-2Ca), is associated with Mn less active nature (-1.182 V) than Ca (–2.868 V).

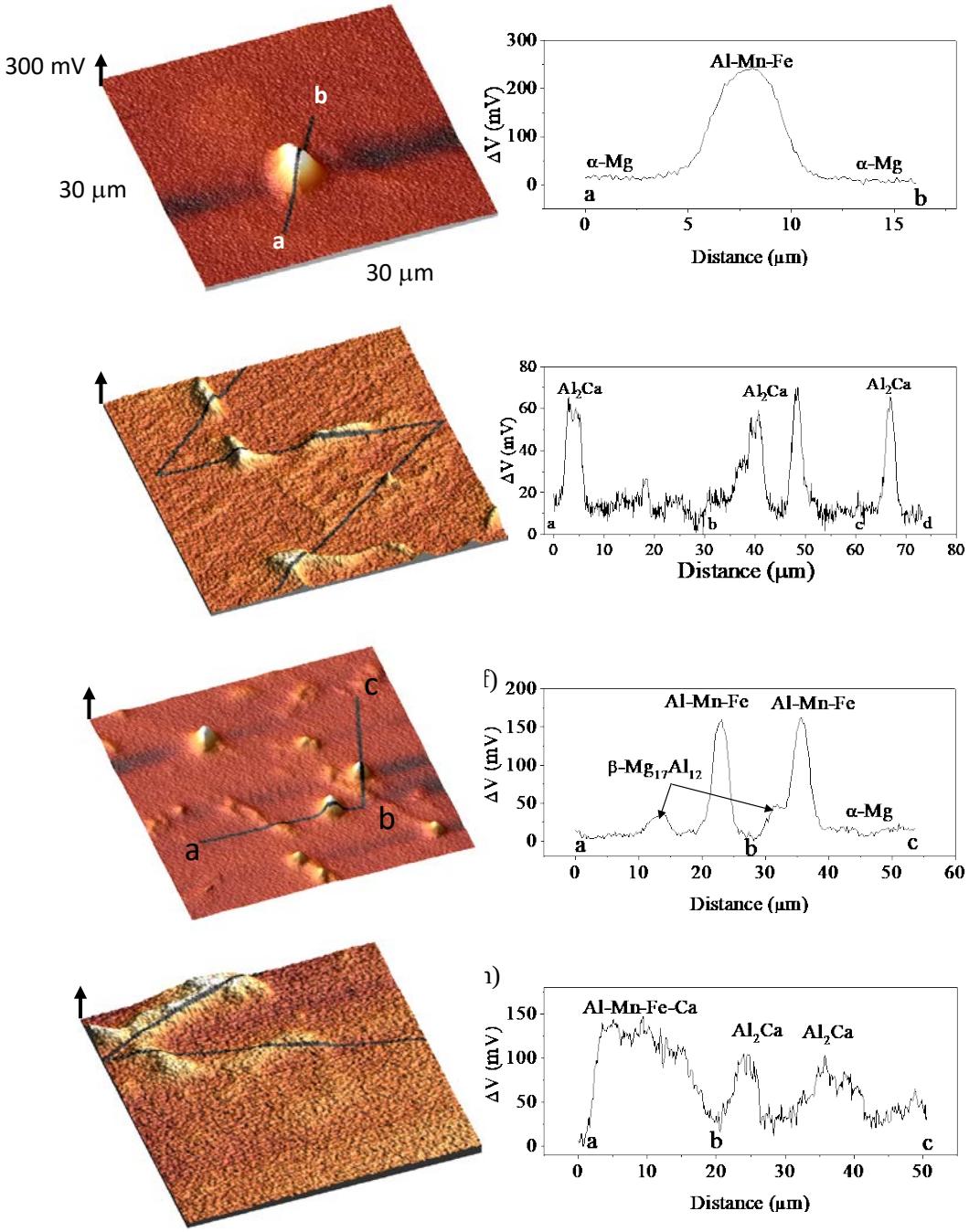
300 mV
30 µm
30 µm
a
b
ΔV (mV)
Al-Mn-Fe
α-Mg
α-Mg
Distance (µm)
Al2Ca
Al2Ca
Al2Ca
c
d
e)
Al-Mn-Fe
Al-Mn-Fe
β-Mg17Al12
α-Mg
f)
Al-Mn-Fe-Ca
Al2Ca
Al2Ca

Figure 5

3.2. Corrosion evaluation

3.2.1. Potentiodynamic polarisation tests

Figure 6 and Table 5 show the potentiodynamic curves and electrochemical parameters of the studied alloys. The reference Mg-9Al alloy shows a corrosion potential, E_{corr}, and corrosion current density, i_{corr}, of -1.472 $V_{Ag/AgCl}$ and 1.0×10^{-4} A cm^{-2}, respectively. The addition of Ca decreases E_{corr} , due its more active nature compared to Mg and shifts the polarisation curves towards lower current densities, reaching minimum values for Mg-9Al-0.5Ca (-1.534 $V_{Ag/AgCl}$ and 5.2×10^{-6} A cm^{-2}). For the latter, the shift of the cathodic branch is larger (Figure 6a). This results in unveiling a clearly defined passive region of approximately 50 mV and a pitting potential of -1.476 V, which is very close to the E_{corr} values of Mg-9Al, Mg-9Al-1Ca and Mg-9Al-2Ca alloys, indicating their higher susceptibility to localized corrosion.

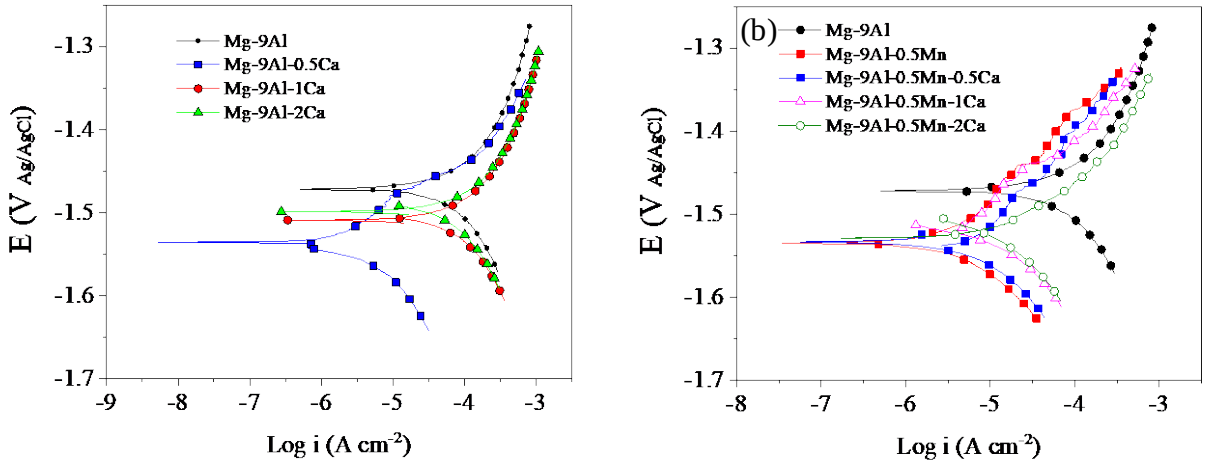

Figure 6

The addition of 0.5 wt.% Mn, Mg-9Al-0.5Mn, (Figure 6b) yields very similar results to those reported for the addition of 0.5 wt.% Ca; E_{corr} and i_{corr} decrease to -1.536 V and 4.9×10^{-6} A cm^{-2}

and a passive region and a pitting potential are revealed. The addition of 0.5 wt.% Ca into the Mn containing alloy (Mg-9Al-0.5Mn-0.5Ca) shows a similar response in terms of E_{corr} and i_{corr} (Table 5). However, further Ca additions (Mg-9Al-0.5Mn-1Ca and Mg-9Al-0.5Mn-2Ca) increase the i_{corr} values (~10^{-5} A cm^{-2}). It can be observed that further additions also result in a slightly increase of the kinetics of the anodic reaction, as it can be deduced from the displacement of the anodic branch towards higher current densities as the content of Ca increases. This could be attributable to the incorporation of Ca to the semi-protective corrosion product layer in the form of Ca-rich compounds such as $Ca(OH)_2$. This compound can be easily dissolved in aqueous media destabilising the oxide film and, thus, decreasing the corrosion resistance (the solubility of $Ca(OH)_2$ is 0.173 g/L while the solubility of $Mg(OH)_2$ is 9.6 ×10^{-4} g/L at 20°C). Despite of this, all the studied Ca-containing alloys show i_{corr} values below that of the Mg-9Al reference alloy.

It is evident from the SKPFM and electrochemical results that the beneficial effects of Ca and Mn are primarily related to a diminishment of the electrochemical activity of cathodic sites and also that minor alloying with Ca (0.5 wt.%) is similar to Mn in terms of the overall electrochemical response. It is also obvious that relatively large Ca additions, 1 and 2 wt.%, are less beneficial or even detrimental. This is most likely due to an increased number of Al_2Ca particles acting as cathodic sites (Figure 7) and, to a lesser extent, due to calcium capacity to activate the anodic reaction (Fig. 6).

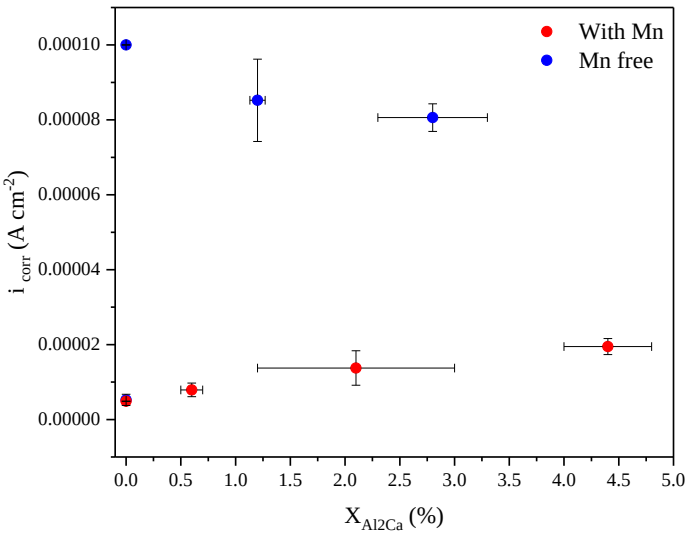

Figure 7

3.3. Hydrogen evolution measurements

Figure 8a shows the volume of hydrogen evolved during the corrosion process as a function of immersion time in 0.5 wt% NaCl. All the materials show linear kinetics, which evidences the poor protective character of the corrosion products formed on the surface of the alloys. In case of Mg-9Al alloy, the specimens start to disintegrate after 3 days of immersion. This behaviour is associated with the high surface Volta potential difference between Fe-rich impurities and the α-Mg matrix, which makes them extremely effective cathodes for microgalvanic corrosion. The incorporation of Ca into these inclusions and into the β-phase reduces the likelihood of severe microgalvanic coupling, thus lowering the corrosion rate. However, this beneficial effect is only significant for the Mg-9Al-0.5Ca alloy. As discussed earlier, this alloy shows higher Ca content in the β-phase than Mg-9Al-1Ca and Mg-9Al-2Ca alloys and does not show precipitation of Al_2Ca

particles. In addition, it has a smaller Fe/Mn ratio. Therefore, the overall electrochemical activity of Mg-9Al-0.5Ca is less than that of Mg-9Al-1Ca and Mg-9Al-2Ca alloys.

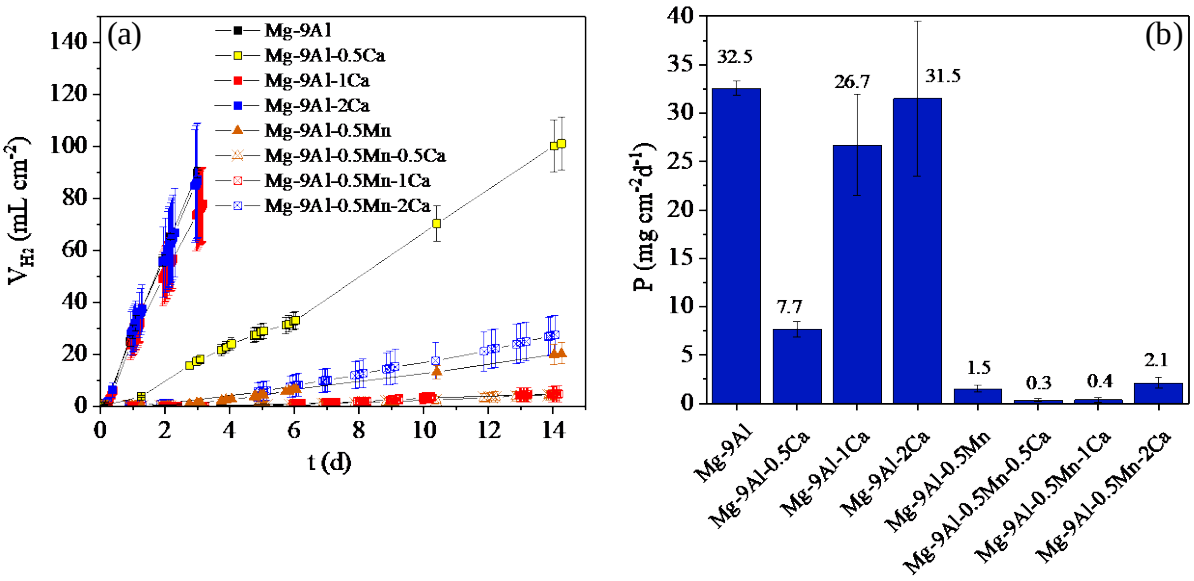

Figure 8

The corrosion rates of Mn-containing alloys are considerably lower than those of Mn-free alloys. This evidences the positive influence of Mn through the *scavenger effect*; the increased amount of Mn in the Al-Mn-Fe impurities reduces significantly their detrimental effect by reducing the Volta potential difference with respect to the matrix. The incorporation of Ca into Mn-containing alloys (Mg-9Al-0.5Mn-0.5Ca) further reduces the corrosion rate, which is associated with decreasing the Volta potential of both Fe-rich inclusions and the β-phase. In case of greater Ca additions, Mg-9Al-0.5Mn-1Ca and Mg-9Al-0.5Mn-2Ca, the formation of new active cathodes (Al_2Ca) and the Ca activation of the anodic reaction show a negative effect, although the corrosion rates are still relatively low. Yang [38] studied the influence of Ca addition (up to 4 wt. %) to Mg-Al alloys and observed that the corrosion rates decrease with additions up to 2 wt. % of Ca, further additions, similarly to this study, resulted in a decrease in the corrosion performance. However, they did not

associate it to the formation of new active cathodes, but to the formation of an anodic $(Mg,Al)_2Ca$ phase acting as a sacrificial anode.

It is worth mentioning that for both sets of alloys, the alloys containing 0.5 % of Ca had the lowest grain size amongst their group; this suggests that smaller grain size also contributes positively to the overall corrosion performance of the alloys. Mg-Al alloys with less than 0.5% Ca (not included in this study) are also expected to outperform Ca-free alloys, but possibly in a lesser extent because Ca incorporation in secondary phases would be less noticeable.

3.3.1. Corrosion morphology

Immersion tests in 0.5 wt. % NaCl solution during 10 min were carried out with the aim of elucidating the most likely locations for corrosion initiation. Ca-free alloys (Mg-9Al and Mg-9Al-0.5Mn) started to corrode at the centre of the primary α-phase (due to its Al content [8]) and near the Fe-rich inclusions which act as effective cathodes (Figure 9a, 9b and 9e). The corrosion propagates rapidly, but slows down when it reaches the β-phase. This barrier effect can be observed more clearly in Figure 10, which shows the cross sections of the specimens after 72h of immersion. In Ca-containing alloys, the locations of corrosion initiation were very similar (Figure 9c, 9d and 9f), although localized corrosion was also observed at the α/Al_2Ca interfaces. Although the corrosion attack around Al_2Ca particles is not that intense, the presence of a greater number of particles leads to a greater number of locations prone to corrosion initiation. This can be clearly observed in Figure 9f. In all the studied materials, regardless of the type and amount of alloying element, corrosion propagates laterally (Figure 10) [39, 40]. Despite being localised, it does not penetrate deep into the metal, due to the β-phase barrier effect, the poor protective nature of the corrosion products film and due to the limited acidification at locations of corrosion preventing pitting corrosion.

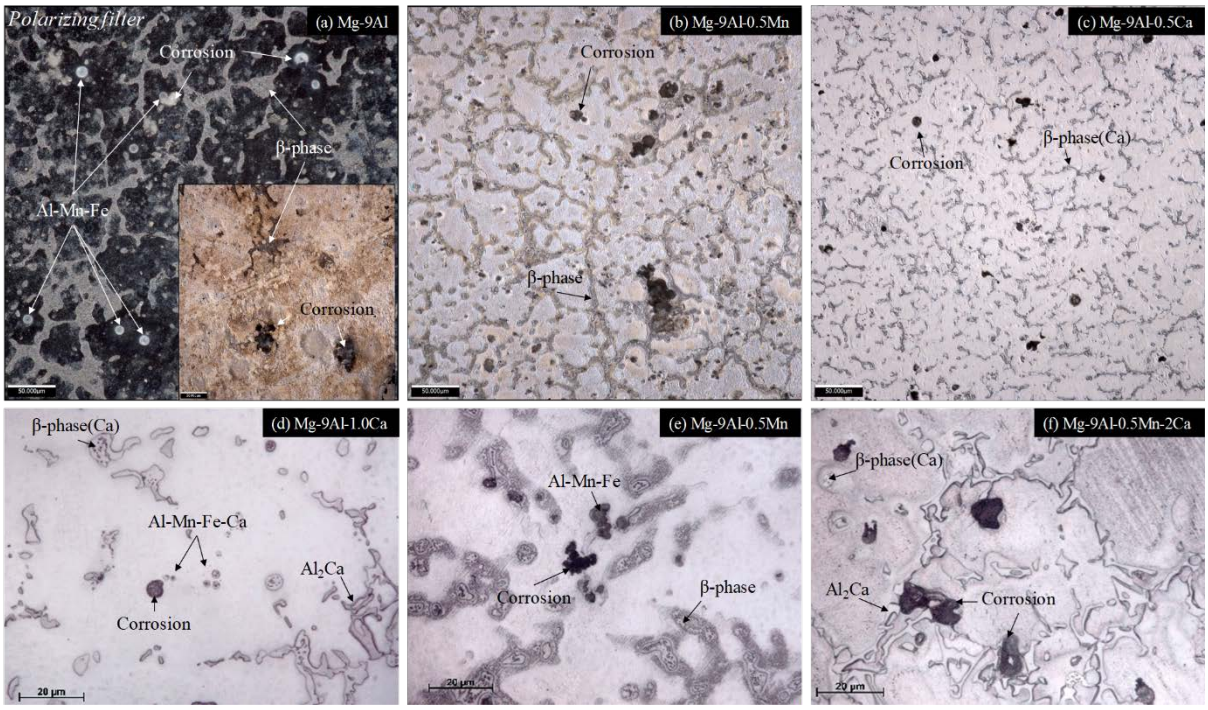
Polarizing filter
(a) Mg-9Al
Corrosion
β-phase
Al-Mn-Fe
Corrosion
(b) Mg-9Al-0.5Mn
Corrosion
β-phase
(c) Mg-9Al-0.5Ca
Corrosion
β-phase(Ca)
β-phase(Ca)
(d) Mg-9Al-1.0Ca
Al-Mn-Fe-Ca
Al2Ca
Corrosion
20 μm
(e) Mg-9Al-0.5Mn
Al-Mn-Fe
Corrosion
β-phase
20 μm
(f) Mg-9Al-0.5Mn-2Ca
β-phase(Ca)
Al2Ca
Corrosion
20 μm

Figure 9

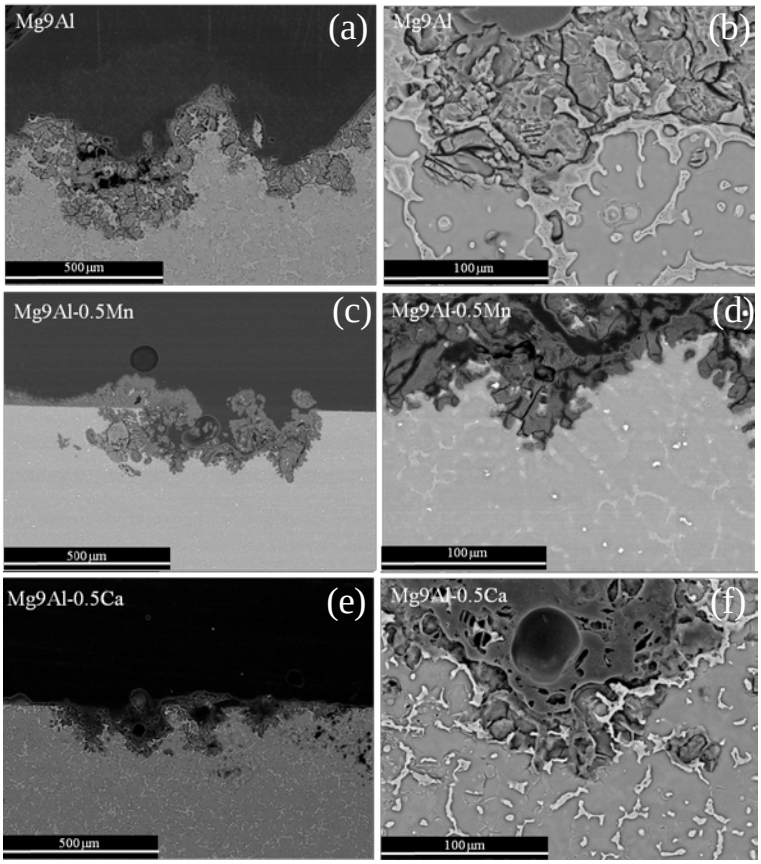

Figure 10

4. Conclusions

- All the studied alloys show an equiaxed grain microstructure with a grain size ranging from ~60 to 150 μm. Ca did not act as a grain refiner. The main effect of Ca was its incorporation into the β-phase and Fe-rich inclusions. Large Ca additions (1 and 2 wt. %) resulted in the precipitation of Al_2Ca intermetallics and a proportional decrease of the area fraction of β-phase.
- SKPFM results revealed that Ca decreases the Volta potential of the β-phase and Fe-rich intermetallics, reaching minimum values of 15-25 mV and 50-100 mV, respectively. This

effect is responsible for decreased cathodic kinetics, as evidenced by electrochemical measurements. However, large Ca additions promote the formation of detrimental Al_2Ca particles, which act as cathodes. Higher additions also activate the anodic reaction, possibly due to Ca incorporation into the semi-passive corrosion product layer in the form of highly soluble compounds.

- Corrosion rates, calculated from H_2 evolution measurements, provided the following ranking from high to low corrosion rates:

  Mg-9Al > Mg-9Al-2Ca > Mg-9Al-1Ca > Mg-9Al-0.5Ca> Mg-9Al0.5Mn-2Ca > Mg-9Al0.5Mn > Mg-9Al-0.5Mn-1Ca > Mg-9Al-0.5Mn-0.5Ca
- In Ca-free alloys, corrosion initiates at the centre of α-Mg grains nearby Fe-rich inclusions, whereas alloys with a high area fraction of Al_2Ca also showed localized corrosion at the α-Mg/Al_2Ca interfaces.

In summary, small Ca additions (<0.5 wt.%) are beneficial for the overall corrosion performance of Mg-Al and Mg-Al-Mn cast alloys, particularly when fast cooling rates are employed.

Acknowledgments

The authors are grateful to MINECO/FEDER (Spain, Project MAT2015-66334-C3-3-R) for financial support. B. Mingo is grateful to The University of Manchester for the award of the Presidential Fellowship and M. Mohedano to MINECO (Spain) for financial support via the Ramon y Cajal Programme (RYC-2017-21843).

Data availability

Data will be made available on request.

References

[1] U. S. Geological Survey Mineral commodity summaries in: U.S.D.o.t. Interior (Ed.), USA, 2017, pp. 105.
[2] V. Schulze, F. Bleicher, P. Groche, Y.B. Guo, Y.S. Pyun, Surface modification by machine hammer peening and burnishing, CIRP Annals, 65 (2016) 809-832.
[3] J. Frayret, J.C. Dupin, S. Pommiers, Corrosion Protection of Magnesium Alloys: From Chromium VI Process to Alternative Coatings Technologies, Magnesium Alloys, (2017) 161.
[4] B. Mingo, Y. Guo, A. Němcová, A. Gholinia, M. Mohedano, M. Sun, A. Matthews, A. Yerokhin, Incorporation of halloysite nanotubes into forsterite surface layer during plasma electrolytic oxidation of AM50 Mg alloy, Electrochimica Acta, 299 (2019) 772-788.
[5] E. Lugscheider, M. Parco, K.U. Kainer, N. Hort.
[6] K. Gusieva, C. Davies, J. Scully, N. Birbilis, Corrosion of magnesium alloys: the role of alloying, International Materials Reviews, 60 (2015) 169-194.
[7] G. Song, A. Atrens, M. Dargusch, Influence of microstructure on the corrosion of diecast AZ91D, Corrosion Science, 41 (1998) 249-273.
[8] R. Arrabal, M. Mohedano, E. Matykina, A. Pardo, B. Mingo, M.C. Merino, Characterization and wear behaviour of PEO coatings on 6082-T6 aluminium alloy with incorporated α-Al2O3 particles, Surface and Coatings Technology, 269 (2015) 64-73.
[9] B. Mingo, R. Arrabal, M. Mohedano, C.L. Mendis, R. del Olmo, E. Matykina, N. Hort, M.C. Merino, A. Pardo, Corrosion of Mg-9Al alloy with minor alloying elements (Mn, Nd, Ca, Y and Sn), Materials & Design, 130 (2017) 48-58.
[10] G. Makar, J. Kruger, Corrosion of magnesium, International materials reviews, 38 (1993) 138-153.
[11] K. Reichek, K. Clark, J. Hillis, Controlling the salt water corrosion performance of magnesium AZ91 alloy, in, SAE Technical Paper, 1985.
[12] O. Lunder, T.K. Aune, K. Nisancioglu, Effect of Mn additions on the corrosion behavior of mould-cast magnesium ASTM AZ91, Corrosion, 43 (1987) 291-295.
[13] H. Matsubara, Y. Ichige, K. Fujita, H. Nishiyama, K. Hodouchi, Effect of impurity Fe on corrosion behavior of AM50 and AM60 magnesium alloys, Corrosion Science, 66 (2013) 203-210.
[14] D. Gandel, N. Birbilis, M. Easton, M. Gibson, Influence of manganese, zirconium and iron on the corrosion of magnesium, Proceedings of corrosion & prevention, (2010) 875-885.
[15] J. Wang, J. Fu, X. Dong, Y. Yang, Microstructure and mechanical properties of as-cast Mg–Al–Sn–Y–Nd alloy, Materials & Design (1980-2015), 36 (2012) 432-437.
[16] Y. Zhang, L. Yang, J. Dai, J. Ge, G. Guo, Z. Liu, Effect of Ca and Sr on the compressive creep behavior of Mg–4Al–RE based magnesium alloys, Materials & Design, 63 (2014) 439-445.
[17] S.-M. Baek, J.S. Kang, H.-J. Shin, C.D. Yim, B.S. You, H.-Y. Ha, S.S. Park, Role of alloyed Y in improving the corrosion resistance of extruded Mg–Al–Ca-based alloy, Corrosion Science, 118 (2017) 227-232.
[18] E. Dabah, G. Ben-Hamu, V. Lisitsyn, D. Eliezer, K. Shin, The influence of Ca on the corrosion behavior of new die cast Mg–Al-based alloys for elevated temperature applications, Journal of materials science, 45 (2010) 3007-3015.
[19] Y.-C. Zhao, M.-C. Zhao, R. Xu, L. Liu, J.-X. Tao, C. Gao, C. Shuai, A. Atrens, Formation and characteristic corrosion behavior of alternately lamellar arranged α and β in as-cast AZ91 Mg alloy, Journal of Alloys and Compounds, 770 (2019) 549-558.

[20] M. Nouri, X. Sun, D.Y. Li, Beneficial effects of yttrium on the performance of Mg–3%Al alloy during wear, corrosion and corrosive wear, Tribology International, 67 (2013) 154-163.
[21] J.I. Kim, H.N. Nguyen, B.S. You, Y.M. Kim, Effect of Y addition on removal of Fe impurity from magnesium alloys, Scripta Materialia, 162 (2019) 355-360.
[22] W. Zhou, N.N. Aung, Y. Sun, Effect of antimony, bismuth and calcium addition on corrosion and electrochemical behaviour of AZ91 magnesium alloy, Corrosion Science, 51 (2009) 403-408.
[23] N.D. Nam, M.Z. Bian, M. Forsyth, M. Seter, M. Tan, K.S. Shin, Effect of calcium oxide on the corrosion behaviour of AZ91 magnesium alloy, Corrosion Science, 64 (2012) 263-271.
[24] I. Apachitei, L. Fratila-Apachitei, J. Duszczyk, Microgalvanic activity of an Mg–Al–Ca-based alloy studied by scanning Kelvin probe force microscopy, Scripta Materialia, 57 (2007) 1012-1015.
[25] A. International, ASTM E112-12 Standard Test Methods for Determining Average Grain Size, in, ASTM International, West Conshohocken, PA, 2012.
[26] I. Horcas, R. Fernández, J. Gomez-Rodriguez, J. Colchero, J. Gómez-Herrero, A. Baro, WSXM: a software for scanning probe microscopy and a tool for nanotechnology, Review of scientific instruments, 78 (2007) 013705.
[27] M. Hurley, C. Efaw, P. Davis, J. Croteau, E. Graugnard, N. Birbilis, Volta potentials measured by scanning Kelvin probe force microscopy as relevant to corrosion of magnesium alloys, Corrosion, 71 (2014) 160-170.
[28] A. Südholz, N. Kirkland, R. Buchheit, N. Birbilis, Electrochemical properties of intermetallic phases and common impurity elements in magnesium alloys, Electrochemical and Solid-State Letters, 14 (2011) C5-C7.
[29] Z. Shi, M. Liu, A. Atrens, Measurement of the corrosion rate of magnesium alloys using Tafel extrapolation, Corrosion Science 52 (2010) 579-588.
[30] B. Mingo, R. Arrabal, M. Mohedano, A. Pardo, E. Matykina, Corrosion and wear of PEO coated AZ91/SiC composites, Surface and Coatings Technology, in press (2016).
[31] P. Li, B. Tang, E.G. Kandalova, Microstructure and properties of AZ91D alloy with Ca additions, Materials Letters, 59 (2005) 671-675.
[32] S.-S. Li, B. Tang, D.-B. Zeng, Effects and mechanism of Ca on refinement of AZ91D alloy, Journal of Alloys and Compounds, 437 (2007) 317-321.
[33] K. Hirai, H. Somekawa, Y. Takigawa, K. Higashi, Effects of Ca and Sr addition on mechanical properties of a cast AZ91 magnesium alloy at room and elevated temperature, Materials Science and Engineering: A, 403 (2005) 276-280.
[34] M. Aljarrah, M. Medraj, X. Wang, E. Essadiqi, A. Muntasar, G. Denes, Experimental investigation of the MgAlCa system, Journal of alloys and compounds, 436 (2007) 131-141.
[35] R. Arrabal, B. Mingo, A. Pardo, E. Matykina, M. Mohedano, M.C. Merino, A. Rivas, A. Maroto, Role of alloyed Nd in the microstructure and atmospheric corrosion of as-cast magnesium alloy AZ91, Corrosion Science, 97 (2015) 38-48.
[36] F. Andreatta, I. Apachitei, A. Kodentsov, J. Dzwonczyk, J. Duszczyk, Volta potential of second phase particles in extruded AZ80 magnesium alloy, Electrochimica Acta, 51 (2006) 3551-3557.
[37] M. Jönsson, D. Thierry, N. LeBozec, The influence of microstructure on the corrosion behaviour of AZ91D studied by scanning Kelvin probe force microscopy and scanning Kelvin probe, Corrosion Science, 48 (2006) 1193-1208.
[38] J. Yang, J. Peng, E.A. Nyberg, F.-s. Pan, Effect of Ca addition on the corrosion behavior of Mg–Al–Mn alloy, Applied Surface Science, 369 (2016) 92-100.

[39] J.G. Brunner, J. May, H.W. Höppel, M.Göken, S. Virtanen, Localized corrosion of ultrafine-grained Al–Mg model alloys, Electrochimica Acta, 55 (2010) 1966-1970.
[40] D. Mercier, J. Światowska, S. Zanna, A. Seyeux, P. Marcus, Role of segregated Iron at grain boundaries on Mg corrosion, Journal of The Electrochemical Society, 165 (2018) C42-C49.

Figure Captions

Figure 1. Optical micrographs of (a) Mg-9Al, (b) Mg-9Al-0.5Ca, (c) Mg-9Al-1Ca, (d) Mg-9Al-2Ca, (e) Mg-9Al-0.5Mn, (f) Mg-9Al-0.5Mn-0.5Ca, (g) Mg-9Al-0.5Mn-1Ca and (h) Mg-9Al-0.5Mn-2Ca alloys, and (i) gran size as a function of Al content in the studied alloys.

Figure 2. SEM micrograph of (a) Mg-9Al, (b) Mg-9Al-0.5Ca, (c) Mg-9Al-1Ca, (d) Mg-9Al-2Ca, (e) Mg-9Al-0.5Mn, (f) Mg-9Al-0.5Mn-0.5Ca, (g) Mg-9Al-0.5Mn-1Ca and (h) Mg-9Al-0.5Mn-2Ca alloys.

Figure 3. (a) XRD diffraction patterns of the studied materials and (b) detail of β-phase diffraction peaks.

Figure 4. (a) Normalised area fraction of β-phase and (b) Al_2Ca as a function of the Ca content.

Figure 5. Surface Volta potential maps and profiles of (a,b) Mg-9Al, (c,d) Mg-9Al-1Ca, (e,f) Mg9Al-0.5Mn and (g,h) Mg-9Al-0.5Mn-1Ca

Figure 6. Polarisation curves of (a) Mn-free and (2) Mn-containing alloys after 1 h of immersion in naturally aerated 0.5 wt.% NaCl solution.

Figure 7. Corrosion current densities as a function of Al_2Ca area fraction.

Figure 8. (a) Hydrogen evolved during the corrosion process as a function of the immersion time and (b) corrosion rates, P, of the studied alloys.

Figure 9. Optical micrographs of (a) Mg-9Al, (b) Mg-9Al-0.5Mn, (c) Mg-9Al-0.5Ca, (d) Mg-9Al-1Ca, (e) Mg-9Al-0.5Mn and (f) Mg-9Al-0.5Mn-2Ca alloys after 10 min of immersion in 0.5 wt. % NaCl.

Figure 10. SEM plan view and cross section of (a) Mg-9Al, (b) Mg-9Al-0.5Mn and (c) Mg-9Al-0.5Ca

Table Captions

Table 1. Chemical composition of the studied alloys.

Table 2. Grain size and area fraction (X_i) measurements of the studied alloys.

Table 3. Phase composition of the studied alloys.

Table 4. Surface Volta potential difference of the main micro constituents of the studied alloys

Table 5. Corrosion potential and current densities of the studied alloys.

Tables

Table 1.

	Elements (wt. %)						Fe/Mn
Alloy	Al	Cu	Ni	Fe	Mn	Ca	
Mg-9Al	12.7	0.00029	<0.0002	0.0155	0.0046	-	3.370
Mg-9Al-0.5Ca	8.7	0.00072	<0.0002	0.0020	0.0235	0.31	0.085
Mg-9Al-1Ca	11.9	0.00352	<0.0002	0.0251	0.039	1.12	0.644
Mg-9Al-2Ca	8.8	0.00253	<0.0002	0.0130	0.033	1.54	0.394
Mg-9Al-0.5Mn	7.3	0.00050	0.0004	0.0110	0.42	-	0.026
Mg-9Al-0.5Mn-0.5Ca	8.4	0.00361	<0.0002	0.0028	0.30	0.36	0.009
Mg-9Al-0.5Mn-1Ca	9.0	0.00219	<0.0002	0.0044	0.40	0.85	0.011
Mg-9Al-0.5Mn-2Ca	10.1	0.00227	<0.0002	0.0058	0.36	1.64	0.016

Table 2.

		Area Fraction (%)		
Alloy	Grain size (μm)	β-phase	Al_2Ca	Al-Mn-Fe (Ca)
Mg-9Al	66±7	15.3±2	-	<0.1
Mg-9Al-0.5Ca	57±3	9.9±0.3	-	<0.1
Mg-9Al-1Ca	112±10	9.9±0.1	1.2±0.01	<0.1
Mg-9Al-2Ca	115±11	6.2±0.3	2.8±0.5	<0.1
Mg-9Al-0.5Mn	115±19	5.8±0.7	-	<0.4
Mg-9Al-0.5Mn-0.5Ca	99±3	5.7±0.5	0.6±0.1	<0.2
Mg-9Al-0.5Mn-1Ca	145±10	4.3±0.1	2.1±0.9	<0.3
Mg-9Al-0.5Mn-2Ca	99±4	4.7±1.0	4.4±0.4	<0.2

Table 3.

Alloy	Phase		Composition (wt. %) Mg	Al	Fe	Mn	Ca
Mg-9Al	α-Mg	Centre	94	6			
		Edge	87	13			
	β-phase		69	31			
	Al-Mn-Fe (Ca)			63	35	1.5	
Mg-9Al-0.5Ca	α-Mg	Centre	96	4			
		Edge	91	9			
	β-phase		66	31			3
	Al_2Ca			73			27
	Al-Mn-Fe (Ca)			88	8	3	1
Mg-9Al-1Ca	α-Mg	Centre	96	94			
		Edge	91	9			
	β-phase		64	34			2
	Al_2Ca			73			27
	Al-Mn-Fe (Ca)			88	8	3	1
Mg-9Al-2Ca	α-Mg	Centre	97	3			
		Edge	91	9			
	β-phase		65	34			1
	Al_2Ca			63			37
	Al-Mn-Fe (Ca)			88	8	3	1
Mg-9Al-0.5Mn	α-Mg	Centre	95	5			
		Edge	89	11			
	β-phase		73	27			
	Al_2Ca						
	Al-Mn-Fe (Ca)			44	2	54	
Mg-9Al-0.5Mn-0.5Ca	α-Mg	Centre	96	4			
		Edge	93	7			
	β-phase		64	34			2
	Al_2Ca			62			38
	Al-Mn-Fe (Ca)			47	1	51	1
Mg-9Al-0.5Mn-1Ca	α-Mg	Centre	97	3			
		Edge	91	9			
	β-phase		67	32			1
	Al_2Ca			63			37
	Al-Mn-Fe (Ca)			46	0.6	53	0.5
Mg-9Al-0.5Mn-2Ca	α-Mg	Centre	97	3			
		Edge	74	24			2
	β-phase		71	28			1
	Al_2Ca			62			38
	Al-Mn-Fe (Ca)			45	0.7	54	0.1

Table 4.

	ΔV (mV)		
Alloy	β-phase	Al_2Ca	Al-Mn-Fe(Ca)
Mg-9Al	30-70	-	250-700
Mg-9Al-0.5Ca	<15	-	50-100
Mg-9Al-1Ca	<25	60-70	50-100
Mg-9Al-2Ca	<25	60-70	50-100
Mg-9Al-0.5Mn	60	-	120-300
Mg-9Al-0.5Mn-0.5Ca	<25	60-70	130-140
Mg-9Al-0.5Mn-1Ca	<25	60-70	130-140
Mg-9Al-0.5Mn-2Ca	<25	60-70	130-140

Table 5.

Alloy	E_{corr} (V)	i_{corr} (A cm^{-2})
Mg-9Al	-1.472±0.001	$(1.0\pm0.7)\times10^{-4}$
Mg-9Al-0.5Ca	-1.534±0.004	$(5.2\pm1.5)\times10^{-6}$
Mg-9Al-1Ca	-1.508±0.001	$(8.5\pm1.1)\times10^{-5}$
Mg-9Al-2Ca	-1.495±0.005	$(8.1\pm0.3)\times10^{-5}$
Mg-9Al-0.5Mn	-1.536±0.001	$(4.9\pm0.1)\times10^{-6}$
Mg-9Al-0.5Mn-0.5Ca	-1.537±0.002	$(7.9\pm1.8)\times10^{-6}$
Mg-9Al-0.5Mn-1Ca	-1.511±0.003	$(1.4\pm0.5)\times10^{-5}$
Mg-9Al-0.5Mn-2Ca	-1.527±0.003	$(1.9\pm2.1)\times10^{-5}$